

Effects of nanoparticles on the stability of polymer fibers

Taejin Kwon and Bong June Sung*

Department of Chemistry, Sogang University, Seoul 04107, Republic of Korea

(Received 3 July 2018; revised manuscript received 8 October 2018; published 31 October 2018)

Polymer fibers, promising materials for tissue engineering and stretchable electronics, are intrinsically unstable due to their large surface-to-volume ratio. Recent experiments revealed that the addition of nanoparticles (NPs) to polymer fibers might enhance their stability. The addition of NPs, however, sometimes increases surface tension, which may facilitate the structural disruption of polymer fibers to polymer globules. It remains, therefore, elusive how NPs would affect the stability and the structural disruption of polymer fibers. In this work, we perform molecular dynamics simulations for polymer fibers with NPs of different types of intermolecular interactions. We prepare unstable polymer fibers that disrupt spontaneously into globules without NPs. We find that upon the addition of NPs, the structural disruption of unstable polymer fibers is hindered and the time (τ_b) taken for the fibers to disrupt to globules is increased. This indicates that the free energy barrier for the transition between the fiber and the globule would be increased due to NPs. The mechanism for the stability enhancement differs for NPs of different intermolecular interactions. When the interaction between polymers and NPs is quite attractive, NPs are located mostly at the center of the fiber around the axis and slow down the polymer mobility. On the other hand, when the interaction between polymers and NPs is not attractive, NPs are likely to be located at the surface of polymer fibers. When NPs are located at the fiber center, τ_b increases with a decrease in temperature. On the other hand, τ_b decreases with a decrease in temperature when NPs are located at the fiber surface.

DOI: [10.1103/PhysRevE.98.042503](https://doi.org/10.1103/PhysRevE.98.042503)**I. INTRODUCTION**

The surface area of soft matter plays an important role in determining the free energy and structure of the soft matter. Especially when its surface-to-volume ratio is large, the soft matter may deform its structure to minimize the surface area and the free energy. For example, polymer fibers with a large surface-to-volume ratio are often unstable, thus deforming spontaneously to polymer globules of smaller surface area. Because polymer fibers are promising materials for various applications such as tissue engineering and stretchable electronics, stabilizing the polymer fibers has been an issue of interest [1–11]. Previous studies suggested that if one were to introduce nanoparticles (NPs) into polymer fibers, the structure of polymer fibers could be manipulated [12–23]. However, how NPs would help stabilize the polymer fibers remains elusive at a molecular level. In this paper, we perform molecular dynamics simulations for unstable polymer fibers and investigate how the addition of NPs could enhance the stability of polymer fibers.

Rayleigh instability explains how cylindrical fluids such as polymer fibers would deform to globules [24,25]. The stability of cylindrical fluids is determined by its initial radius (R_0) and the wave number (k) of the disturbance on the fluid surface [26–37]. If $kR_0 < 1$, the cylindrical fluid should break into small globules. In this study, we prepare polymer fibers, of which kR_0 is comparable to or slightly smaller than 1. The polymer fibers in our simulations are, therefore, unstable without NPs and deform spontaneously into globules. The

surface tension and viscosity of polymer fibers also influence the stability of polymer fibers. Polymer fibers of a larger surface tension are more susceptible to the perturbation to the polymer fibers. On the other hand, polymers of larger viscosity tend to dampen the perturbation, which slows down the deformation [25,38,39].

The addition of NPs may influence both the surface tension and the viscosity of polymer fibers. Previous studies reported that when NPs were dispersed in fluids, the viscosity and the surface tension of fluids were controlled [13,15,19,21,40,41]. Hoogesteijn von Reitzenstein *et al.* showed that the morphology of electrospun polymer fibers could be controlled by changing concentration of metal oxide NPs [41]. A high concentration of metal oxide NPs increased both the surface tension and viscosity of polymer solution, thus leading to transitions between different morphologies. Mazinani *et al.* also showed that the addition of carbon nanotubes would help manipulate the morphology of the polystyrene fibers. Because the large surface tension facilitates the disruption of fibers and the large viscosity slows down the disruption, tuning the surface tension and the viscosity should be critical to stabilizing the polymer fibers. In this paper, we introduce various types of NPs into unstable polymer fibers and investigate how the intermolecular interactions between NPs and polymers affect the stability.

The spatial arrangement of NPs is dependent on the interaction between NPs and polymers. A previous simulation study for polymer films showed that when the intermolecular interactions between NPs and polymers were quite attractive, NPs were located mostly at the center of polymer films [42]. On the other hand, when the interactions between NPs and polymers were quite repulsive, NPs were located at the interfacial region of the polymer films. In this work, we

*bjsung@sogang.ac.kr

also find that the NPs of attractive interactions are located at the fiber center around the fiber axis, while the NPs of relatively repulsive interactions are located at the interfacial region of the polymer fibers. Previous studies showed that the arrangement of NPs in fluid vesicles affected the curvature energy [43–45]. We also find from our simulations that the mechanism for the stabilization would depend on the spatial arrangement of NPs.

The rest of the paper is organized as follows. In Sec. II we describe the simulation model and methods. In Sec. III we present the simulation results and discussions, and in Sec. IV we summarize and conclude our study.

II. MODEL AND METHODS

We employ a coarse-grained but generic model to simulate polymers and NPs. Polymers are modeled as bead-spring chains of $N = 32$ monomers of mass m , which has been often used in previous studies [42,46–51]. The nonbonding interaction U_{pp} between two nonbonded monomers is described by a truncated and shifted Lennard-Jones (LJ) potential:

$$U_{pp}(r) = 4\epsilon \left[\left(\frac{\sigma}{r} \right)^{12} - \left(\frac{\sigma}{r} \right)^6 \right] - \epsilon_c, \quad r < r_c. \quad (1)$$

Here r denotes the distance between two monomers, and σ is the monomer diameter that is used as the length unit. ϵ is the energy unit in our study and the product of Boltzmann constant (k_B) and temperature (T): $\epsilon = k_B T$, $r_c = 2.5\sigma$, and $\epsilon_c = 4\epsilon \left[\left(\frac{\sigma}{r_c} \right)^{12} - \left(\frac{\sigma}{r_c} \right)^6 \right]$. The bonding interaction between two bonded monomers is described by a harmonic potential (U_b),

$$U_b(r) = K_b(r - r_0)^2, \quad (2)$$

where $K_b = 1000\epsilon/\sigma^2$ and $r_0 = 1\sigma$.

A NP is modeled as a sphere of mass m and diameter $\sigma_n = 3\sigma$. We also employ the truncated and shifted LJ potential to describe the nonbonding interaction $U_{np}(r)$ between a NP and a monomer as

$$U_{np}(r) = 4\epsilon_{np} \left[\left(\frac{\sigma_{np}}{r} \right)^{12} - \left(\frac{\sigma_{np}}{r} \right)^6 \right] - \epsilon_{cn}, \quad r < r_{cn}. \quad (3)$$

Here $\sigma_{np} = (\sigma + \sigma_n)/2$ and $r_{cn} = 2.5\sigma_{np}$. The interaction parameter (ϵ_{np}) between the NP and the monomer varies in this study from 1 to 3ϵ . As ϵ_{np} is increased, the interaction between the NP and the monomer becomes more attractive: $\epsilon_{cn} = 4\epsilon_{np} \left[\left(\frac{\sigma_{np}}{r_{cn}} \right)^{12} - \left(\frac{\sigma_{np}}{r_{cn}} \right)^6 \right]$. The interaction between NPs is also described by the same type of the truncated and shifted LJ potential but with a different set of the interaction parameter ($\epsilon_{nn} = \epsilon$), the interaction diameter (σ_n), and the cutoff distance ($2.5\sigma_n$).

We prepare an unstable polymer fiber in order to investigate how NPs would improve the stability of the unstable polymer fiber [47]. First, we place 240 polymer chains at random positions in a rectangular simulation box with periodic boundary conditions applied in all directions. If there is any overlap between particles, the particles are inserted at different random positions. The dimensions of the rectangular simulation box are $(L_x, L_y, L_z) = (48\sigma, 12.65\sigma, 12.65\sigma)$ such that the monomer number density is 1. When we need to insert NPs into the system, we avoid the overlap between NPs and other particles, and insert 53 NPs. We perform molecular dynamics

(MD) simulations and equilibrate the system in the rectangular simulation box. We use the Nose-Hoover thermostat and the velocity-Verlet integrator with a time step of $\delta t = 0.01$.

Once the equilibrium configurations in the rectangular simulation box are obtained, we increase the values of both L_y and L_z to 200σ in order to construct a polymer fiber. The periodic images of a polymer along y and z directions cannot interact with one another. The polymer fiber is unstable because $kR_0 = (2\pi/L_x) \times (15.30/2) \approx 1$. In order to relax the polymer conformations in the unstable polymer fiber, we impose a virtual cylindrical wall that wraps and confines the polymer fiber and perform MD simulations. A repulsive Weeks-Chandler-Andersen (WCA) interaction is applied between the wall and the particles of the polymer fiber. We propagate the system (with a cylindrical wall) until the time correlation functions of the bond vector of polymers decay.

We estimate the density distribution functions [$\rho_r(r)$ and $\rho_a(x)$] along the radial and axial directions by using $\rho_r(r) = \langle \frac{1}{2\pi r} \delta(r - d_m) \rangle$ and $\rho_a(x) = \langle \delta(x - x_m) \rangle$. Here d_m denotes the shortest distance between a monomer and the fiber axis, and x_m is the x position of the monomer; $\langle \dots \rangle$ denotes an ensemble average. Figure 1(a) depicts a representative radial monomer density distribution function $\rho_r(r)$ for the polymer fiber without any NPs at $T = 1$ right after the polymer fiber is

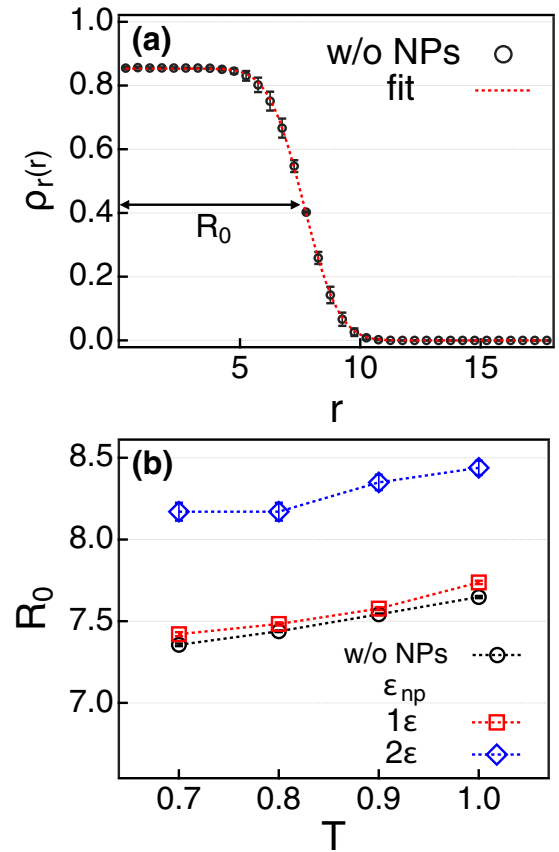


FIG. 1. (a) The simulation results for the monomer density distribution function [$\rho_r(r)$] for a polymer fiber without any NPs as a function of the shortest distance (r) from the fiber axis. The dotted line is a fit to simulation results. (b) The initial radii (R_0) of polymer fibers without and with NPs for various temperature.

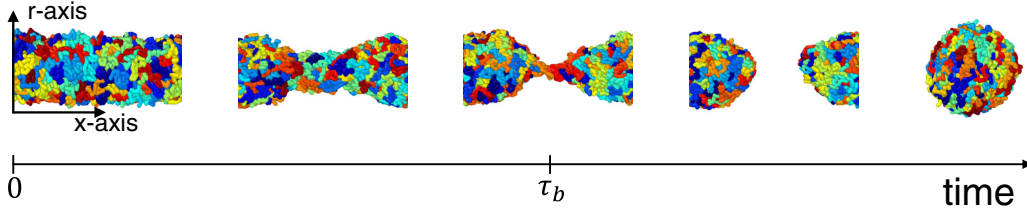


FIG. 2. Representative simulation snapshots for the disruption of an unstable polymer fiber without NPs to a globule. Different polymer molecules are represented using different colors. τ_b is a characteristic time when the polymer fiber begins to be broken.

equilibrated inside a repulsive cylindrical wall. The monomer density is uniform with $\rho_r(r) \approx 0.85$ around the fiber axis. When the distance to the fiber axis is 5σ or larger, $\rho_r(r)$ begins to decay.

The monomer density of $\rho_r(r) \approx 0.85$ around the fiber axis is much larger than the critical overlap concentration (≈ 0.36) of our polymer chains. The critical overlap concentration is obtained by calculating the number of monomers of a polymer within the pervaded volume of the single chain. The pervaded volume is estimated as $4/3\pi R_g^3$ and R_g is the radius of gyration of a polymer chain in our simulations. The polymer chain of $N = 32$ is too short to entangle other polymers. However, the monomer density at the fiber axis is so large that polymers penetrate the pervaded volume of other polymers. On the other hand, recent simulation studies suggested that the extent of entanglement of polymers would be diminished under geometric confinements such as polymer fibers and films ([52,53]). Therefore, molecular simulations with short chains would be a good starting point to investigate the effects of NPs on the polymer fibers.

In order to estimate the initial radius (R_0) and the interface width (w), we fit the simulation results for $\rho_r(r)$ to a hyperbolic tangent function of $\rho_r(r) = \frac{\rho_c}{2} [1 + \tanh(\frac{R_0 - r}{w})]$. Here ρ_c denotes the value of $\rho_r(r)$ at $r = 0$. Figure 1(b) depicts the initial value (R_0) of the fiber radius as a function of T with and without NPs. R_0 increases with an increase in T regardless of the presence of NPs. When the interaction between NPs and polymers is quite attractive with $\epsilon_{np} = 2\epsilon$, R_0 is increased by about 10% compared to the polymer fibers without NPs. As shall be discussed below, the increase in R_0 for $\epsilon_{np} = 2\epsilon$ is attributed to the fact that all NPs are located at the fiber center around the axis. On the other hand, when $\epsilon_{np} = 1\epsilon$ and the interaction is not very attractive, R_0 of the polymer fibers is comparable to that of polymer fibers without NPs.

Regardless of the presence of NPs, the values of kR_0 is smaller or comparable to 1 for all polymer fibers in our simulations. For example, in the case of $T = 1$ and $\epsilon_{np} = 2\epsilon$, R_0 for the polymer fiber is the largest around $R_0 = 8.4\sigma$ [Fig. 1(b)]. Because $k = 2\pi/L_x$ in our simulations, $kR_0 \approx 1.1$. According to Plateau and Rayleigh [24,25], all polymer fibers prepared in our simulations are unstable and expected to disrupt to globules spontaneously.

The monomer of coarse-grained models for polymers usually corresponds to the Kuhn monomer of polymers. In the case of polyethylene, the Kuhn length is about 14 Å. The diameter of polymer fibers in our simulations is, therefore, about $15\sigma = 21$ nm. There have been various experiments where nanofibers of diameter around 20 nm were prepared.

For example, Park *et al.* synthesized the nanofibers made of polyacetylene, of which the diameter was down to 20 nm [54], and Zhou *et al.* also reported nanofibers made of polyaniline [55]. The diameter of their nanofibers was as low as 20 nm.

In order to estimate how long it takes for the polymer fibers to disrupt to globules, we investigate the density distribution function [$\rho_a(x)$] along the axis. At time $t = 0$, we remove the repulsive cylindrical wall that wraps the polymer fiber and begin to propagate the system by performing MD simulations, and then we estimate $\rho_a(x)$ at different times. When $t = 0$, $\rho_a(x)$ is uniform as expected. As time goes on, $\rho_a(x)$ continues to fluctuate. After some time $t = \tau_b$, we may observe that $\rho_a(x) = 0$ at a certain value of x , i.e., there is no monomer at the position x and the fiber is broken. The time τ_b is defined as the breakup time for the polymer fiber (Fig. 2). We perform 30 different MD simulations and average τ_b over those trajectories.

In order to investigate how NPs of different types of interactions would affect the polymer mobility, we investigate the mobility and the mean-square displacement of monomers in polymer fibers while the fiber morphology is still retained after the removal of the repulsive cylindrical wall. We investigate the mean-square displacement [$\langle(\Delta x)^2(t)\rangle = \langle|x(t) - x(0)|^2\rangle$] of monomers along the fiber axis. Here $x(t)$ is the x position of a monomer at time t . We also estimate monomer mobilities (M_a and M_r) along the axial and radial directions. M_a is the average displacement of monomers along the axis during $t = 1000$, i.e., $M_a \equiv \langle|x(t = 1000) - x(0)|\rangle$. It usually takes about $t = 1000$ for a monomer to diffuse along the axis by the size of NPs. Similarly, the radial mobility (M_r) of monomers is defined as $M_r \equiv \langle\sqrt{[y(t = 1000) - y(0)]^2 + [z(t = 1000) - z(0)]^2}\rangle$. We estimate M_a and M_r for monomers at both the interfacial region and the fiber center. If the distance between a monomer and the fiber axis is less than 1σ , the monomer is determined to be at the center. If the distance is about R_0 , the monomer is considered as being at the surface.

III. RESULTS AND DISCUSSIONS

A. The deformation kinetics of polymer fibers

Polymer fibers in our simulations are unstable with kR_0 comparable to 1 such that polymer fibers deform to globules spontaneously. The free energy difference [$\Delta F \equiv F(\text{globule}) - F(\text{fiber})$] between the globule and the fiber is, therefore, negative (Fig. 3). Because the deformation to globules should accompany large structural fluctuations of the

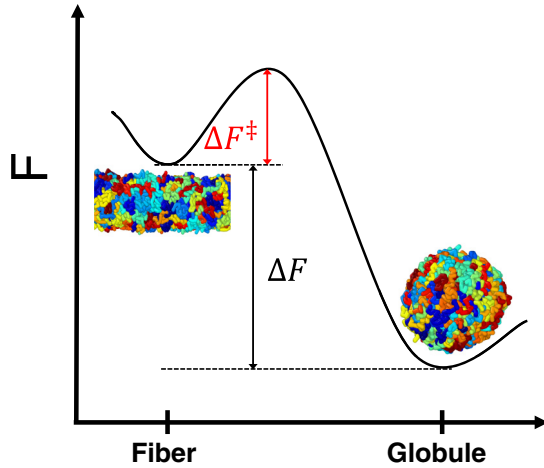


FIG. 3. The schematic for a free energy (F) diagram for the fiber deformation. In our simulations polymer fibers with $kR_0 \leq 1$ are unstable such that $\Delta F < 0$. ΔF^\ddagger is the free energy barrier for the polymer fibers to deform to globules.

polymer fiber, there should be a free energy barrier (ΔF^\ddagger) that the polymer fiber has to overcome for the deformation. If ΔF^\ddagger were to be increased somehow, it would take more time for the deformation to occur.

We investigate how the unstable polymer fiber deforms to globules by monitoring the temporal evolution of the thinnest radius (\bar{r}_m) of the polymer fiber. We estimate \bar{r}_m as follows. First, we calculate the radius ($\bar{r}(x)$) at a given position x along the fiber axis. $\bar{r}(x)$ is the first moment of the density distribution function along the radial direction at a given position x , i.e., $\bar{r}(x) = \int_0^\infty r \rho_r(x, r) dr$. \bar{r}_m is then the minimum value of $\bar{r}(x)$.

We remove the repulsive cylindrical wall at time $t = 0$, propagate the system by performing MD simulations, and measure \bar{r}_m as a function of time t . Figure 4 depicts \bar{r}_m as a function of $\tau_b - t$. Note that time t progresses from right to left in the figure. After \bar{r}_m keeps fluctuating for a while

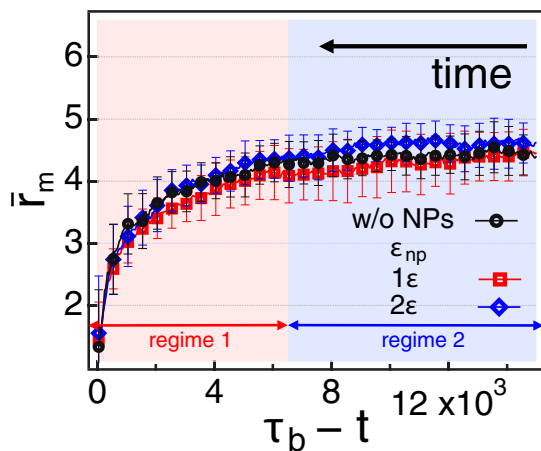


FIG. 4. The temporal evolution of the minimum radius \bar{r}_m of polymer fibers without any NPs (black) and with NPs of $\epsilon_{np} = 1\epsilon$ (red) and $\epsilon_{np} = 2\epsilon$ (blue). τ_b is the breakup time for the polymer fiber. Time progresses from right to left.

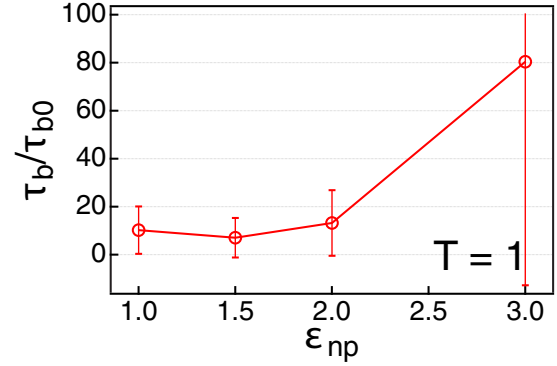


FIG. 5. Simulation results for τ_b divided by its value (τ_{b0}) for the polymer fiber without NPs as a function of ϵ_{np} for $T = 1$.

in *regime 2*, \bar{r}_m begins to decay to zero in *regime 1* and the polymer fiber is eventually broken at $t = \tau_b$. The length of regime 2 (where \bar{r}_m fluctuates) differs for different trajectories. On the other hand, the length of regime 1 (where \bar{r}_m decays) hardly changes with trajectories. More interesting is that even when we introduce NPs to the polymer fibers, the length of regime 1 is not changed. As shown in Fig. 4, \bar{r}_m overlaps with one another in regime 1 regardless of the presence and the type of NPs, i.e., the breakup time of polymer fibers in our simulations is determined by the duration of regime 2. This might be attributed to the fact that once the polymer fiber crosses the free energy barrier (ΔF^\ddagger), the deformation occurs quite quickly regardless of NPs. On the other hand, the length of regime 2 is sensitive to the presence and the type of NPs. This implies that one might increase ΔF^\ddagger by adding NPs, which increases the length of regime 2 and make the polymer fiber kinetically stable.

As NPs are added to the polymer fiber, τ_b is increased significantly and the polymer fiber becomes kinetically stable. Figure 5 depicts the relative value of τ_b , i.e., τ_b divided by its value (τ_{b0}) for polymer fibers without NPs. At $T = 1$ as shown in Fig. 5, τ_b is increased by up to a factor of 80. In other words, it takes 80 times longer for the polymer fiber to disrupt to polymer globules when NPs of $\epsilon_{np} = 3\epsilon$ are added. As ϵ_{np} is increased and the interaction between NPs and polymers becomes more attractive, τ_b is increased. This indicates that one may enhance the stability of fibers significantly by adding NPs. At a lower temperature of $T = 0.7$, the polymer fiber becomes more kinetically stable as NPs are added. In case of $\epsilon_{np} = 2\epsilon$, 90% polymer fibers of our simulations do not break down even until $t = 1.5 \times 10^6$, implying that the polymer fibers with those NPs become very stable.

Note that the error bars are quite large in this study, especially for large τ_b , which is because there are a few trajectories for each set of parameters where it takes exceptionally long for the polymer deformation. We estimate the distribution functions [$P(\tau_{b,i}/\tau_b)$] of breakup times ($\tau_{b,i}$) of individual trajectories [divided by their average value (τ_b)]. We find that regardless of ϵ_{np} , $P(\tau_{b,i}/\tau_b)$ is exponential (Fig. 6). Exponential distributions usually indicate that the error in τ_b increases with an increase in τ_b . This leads to a very large error for $\epsilon_{np} = 3\epsilon$ in Fig. 5.

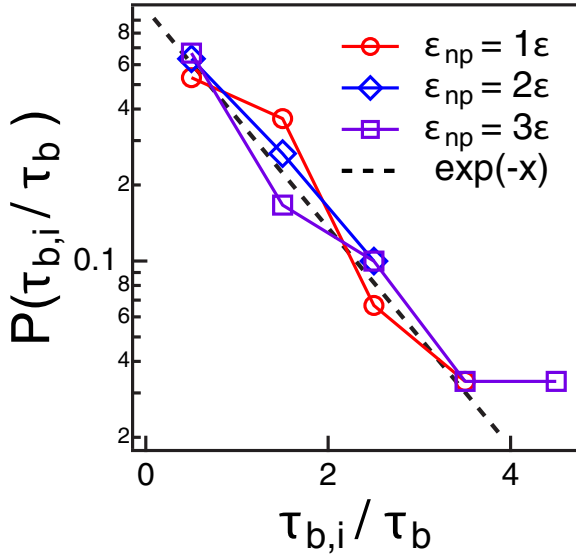


FIG. 6. Simulation results for the distribution of the breakup time ($\tau_{b,i}$) of an individual trajectory divided by its average value (τ_b) for $T = 1$ and different values of ϵ_{np} .

The deformation kinetics of polymer fibers depends on temperature (T) but in different fashions depending on the interaction types of NPs. Figure 7 depicts τ_b of polymer fibers with and without NPs as a function of T . Without any NP in the polymer fiber, τ_b is not very sensitive to T . As T is decreased, the error in τ_b is increased because there are a few trajectories where it takes quite a long time for the polymer fiber to be broken. However, the average value of τ_b is increased only slightly by about 20% as T is decreased from 1 to 0.7 [Fig. 7(a)]. When NPs are added to the polymer fibers, the temperature dependence of τ_b depends on the interaction type. When the interaction between NPs and monomers is quite attractive with $\epsilon_{np} = 2\epsilon$, τ_b is increased by more than a factor of 4 as T is decreased to 0.8 [Fig. 7(c)]. On the other hand, when the interaction is not very attractive with $\epsilon_{np} = 1\epsilon$, τ_b is rather decreased by about 50% as T is decreased to 0.7.

Such different temperature dependences of τ_b imply that the polymer fiber would be stabilized via different mechanisms depending on the interaction types of NPs. Because τ_b is determined mainly by regime 2 (where the polymer fiber fluctuates before crossing the free energy barrier), $\tau_b \sim \exp(\Delta F^\ddagger/k_B T) = \exp(\Delta E^\ddagger/k_B T) \exp(-\Delta S^\ddagger/k_B)$, where ΔE^\ddagger and ΔS^\ddagger denote the differences in the internal energy and the entropy between the polymer fiber and the transition state for the deformation, respectively. The temperature dependence is expected to increase due to the energetic contribution ($\Delta E^\ddagger/k_B T$) to τ_b . When $\epsilon_{np} = 2\epsilon$, τ_b increases with an increase in $1/T$ such that $\Delta E^\ddagger > 0$. On the other hand, when $\epsilon_{np} = 1\epsilon$, τ_b decreases with an increase in $1/T$ such that $\Delta E^\ddagger < 0$.

In our simulations, however, it is a formidable task to estimate the values of ΔE^\ddagger because the determination of the configurations of polymer fibers at the transition state is not possible. Such different temperature dependence of τ_b (and

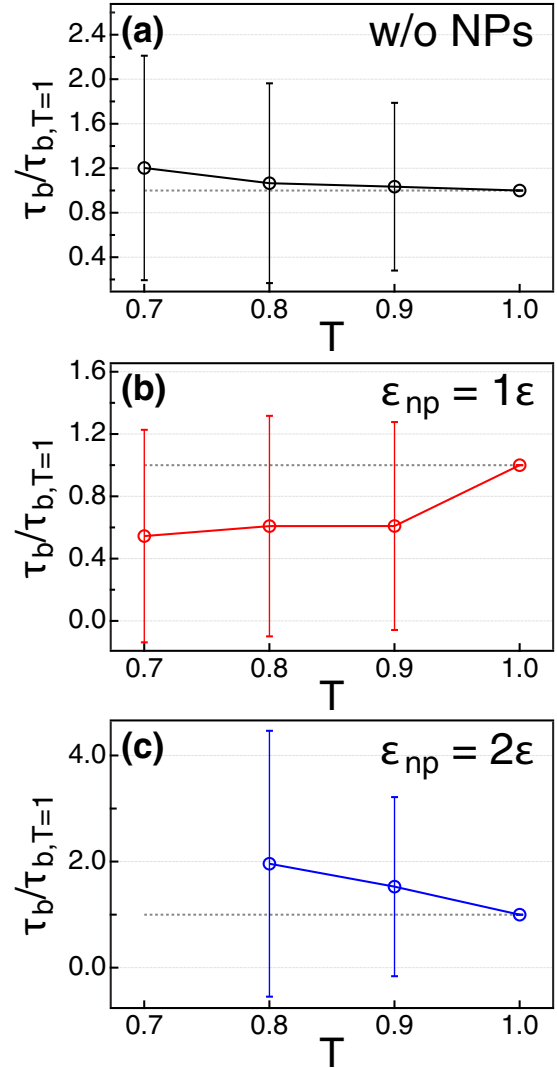


FIG. 7. Simulation results for τ_b divided by its value at $T = 1$ as a function of temperature T for the polymer fiber (a) without NPs and with NPs of (b) $\epsilon_{np} = 1\epsilon$ and (c) $\epsilon_{np} = 2\epsilon$. Note that the error bars are larger at a lower temperature because it takes quite a long time for some polymer fibers to break up at a lower temperature.

different values of ΔE^\ddagger) may relate to the spatial arrangement of NPs. NPs of different values of ϵ_{np} are distributed in different manners within polymer fibers, which is discussed in following sections.

B. The spatial arrangement of NPs within polymer fibers

The spatial arrangement of NPs inside polymer fibers depends strongly on the interaction strength (ϵ_{np}) between NPs and polymers. Figure 8 depicts the radial density distribution functions of both NPs [$\rho_n(r)$] and monomers [$\rho_r(r)$] as a function of the shortest distance (r) from the fiber axis. $\rho_n(r)$ and $\rho_r(r)$ are calculated in our MD simulations, while the polymer fiber structure is retained before breakup. Note that $r = 0$ corresponds to the center of the polymer fiber. When $\epsilon_{np} = 1\epsilon$ and the interaction is not very attractive between NPs and polymers, NPs are located mostly at the interfacial region of the polymer fiber. ρ_n has a single peak around $r = 8\sigma$

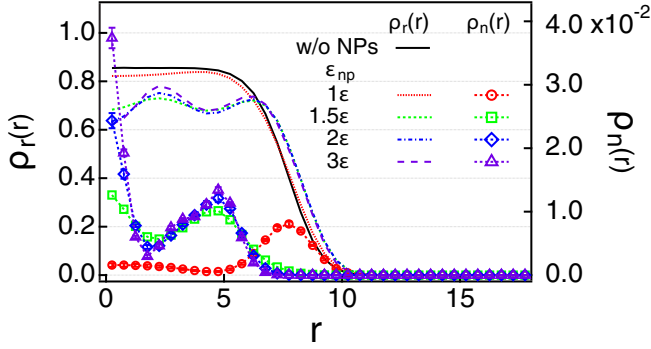


FIG. 8. The density distribution functions of monomers [$\rho_r(r)$, lines] and NPs [$\rho_n(r)$, symbols] as a function of the distance r from the fiber axis for various values of ϵ_{np} .

for $\epsilon_{np} = 1\epsilon$. On the other hand, as ϵ_{np} is increased and the interaction becomes more attractive, NPs are more likely to be placed inside the polymer fiber. In the case of $\epsilon_{np} = 2\epsilon$, for example, $\rho_n(r)$ has two peaks at $r \approx 5$ and 0σ . As ϵ_{np} is increased from 1.5 to 3ϵ , the peak at $r = 0$ is increased, which indicates that more NPs are located at the fiber center for higher ϵ_{np} . Such a dependence of NP arrangement on the interaction strength has been also reported for thin polymer films [42].

The spatial arrangement of NPs affects the initial radius (R_0) of a fiber [Fig. 1(b)]. As shown in Fig. 8, when NPs are located mostly at the interfacial region ($\epsilon_{np} = 1\epsilon$), the monomer density distribution function [$\rho_r(r)$] is almost identical to that of polymer fibers without any NPs. Therefore, R_0 hardly changes upon addition of NPs of $\epsilon_{np} = 1\epsilon$. On the other hand, when the interaction between NPs and polymers is attractive with $\epsilon_{np} \geq 1.5\epsilon$, NPs are located at the central region of the polymer fiber such that monomers are depleted relatively around the fiber axis. This leads to a slight increase in R_0 of the polymer fibers.

Previous experiments reported that poor dispersion of NPs might make polymer fibers unstable [13,40]. In order to investigate dispersion of NPs in our systems, we calculate the radial distribution function of NPs, i.e., $g(r) = \frac{V}{N_n^2} < \sum_i \sum_j \delta(r_{ij} - r) >$. Here r_{ij} is the distance between the i th and j th NPs, and N_n and $V = \pi R_0^2 L_x$ denote the number of NPs and the estimated volume of polymer fibers. As shown in Fig. 9, when $\epsilon_{np} = 1\epsilon$, $g(r)$ does not have a sharp peak, thus indicating that NPs are well dispersed at the interfacial region of the polymer fiber. On the other hand, when $\epsilon_{np} = 2\epsilon$, $g(r)$ has a high peak at $r \approx 6\sigma$ (about the NP diameter). This is because NPs are located mostly at the fiber center around the axis. The peak height of $g(r = 6\sigma) \approx 2.5$ is, however, not very large, such that NPs in our simulations for $\epsilon_{np} = 2\epsilon$ are still dispersed well inside the polymer fiber. Moreover, NPs of $\epsilon_{np} = 2\epsilon$ make the polymer fiber more kinetically stable in our study, which indicates that the destabilization of the polymer fiber due to the poor dispersion is not observed in our simulations.

C. The mobility of polymer fibers with NPs embedded

Not only the free energy barrier (ΔF^\ddagger) but also the bulk viscosity may affect the time (τ_b) taken for the polymer

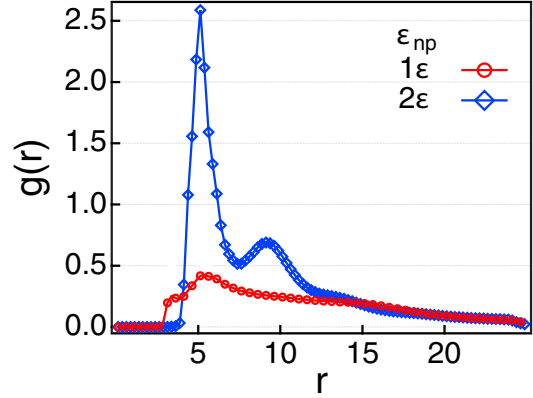


FIG. 9. The radial distribution function [$g(r)$] of NPs for $\epsilon_{np} = 1\epsilon$ and 2ϵ .

fiber to disrupt. If the bulk viscosity would be increased (for example, due to a decrease in temperature), the mobility of monomers would be decreased such that the translation and conformational change of polymers would slow down. We find from our simulations that NPs slow down the polymer mobility. Figure 10 depicts the mean-square displacement [$\langle (\Delta x)^2(t) \rangle$] of monomers along the fiber axis (the x direction) with and without NPs. $\langle (\Delta x)^2(t) \rangle$ is linear with time t at long times such that monomers in our simulations show Fickian diffusion along the fiber axis. As NPs are introduced, $\langle (\Delta x)^2(t) \rangle$ is decreased, implying that the monomer mobility is decreased. As ϵ_{np} is increased, $\langle (\Delta x)^2(t) \rangle$ is decreased even further. In the case of $\epsilon_{np} = 3\epsilon$ where the interaction between NPs and monomers is the most attractive, $\langle (\Delta x)^2(t) \rangle$ is smaller by about 40% than polymer fibers without NPs. This indicates that the viscosity of polymer fibers should be increased upon the addition of NPs.

We find that the effects of NPs on the monomer mobility depend on the interaction strength (ϵ_{np}) and the spatial arrangement of NPs. We estimate the axial (M_a) and radial (M_r) mobility of monomers. The mobility in this study is defined as the magnitude of the displacement of

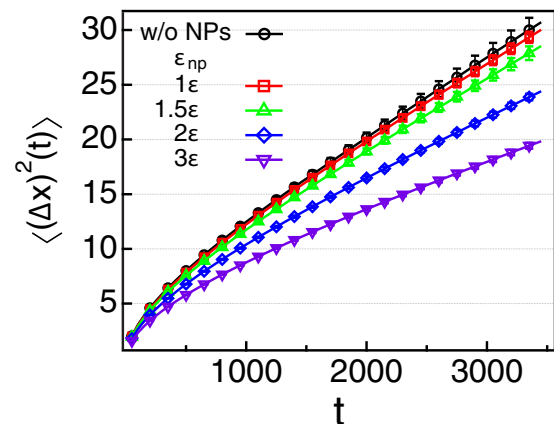


FIG. 10. The mean-square displacement [$\langle (\Delta x)^2(t) \rangle$] of monomers along the polymer fiber axis for various ϵ_{np} .

TABLE I. The relative mobility of monomers of polymer fibers for $\epsilon_{np} = 1\epsilon$ and 2ϵ at $T = 1$.

		NPs at the surface ($\epsilon_{np} = 1\epsilon$)	NPs at the center ($\epsilon_{np} = 2\epsilon$)
Monomers at the center	$M_r/M_{r,0}$	0.999 (± 0.017)	0.891 (± 0.015)
	$M_a/M_{a,0}$	1.00 (± 0.019)	0.88 (± 0.017)
Monomers at the surface	$M_r/M_{r,0}$	0.90 (± 0.14)	0.85 (± 0.13)
	$M_a/M_{a,0}$	0.988 (± 0.014)	0.932 (± 0.014)

monomers during $t = 1000$ along either the axial or radial direction. We also categorize monomers into two groups: monomers at the fiber center and monomers at the interfacial region. We find from our simulations that the mobility of monomers is affected by NPs in a complicated fashion.

When NPs are located mostly at the interfacial region (i.e., when $\epsilon_{np} = 1\epsilon$), the mobility of monomers at the center is hardly affected by the presence of NPs along both the radial and axial directions. Table I depicts the relative mobility (either $M_a/M_{a,0}$ or $M_r/M_{r,0}$) defined as the ratio of mobility of monomers with and without NPs. Here $M_{r,0}$ and $M_{a,0}$ denote the mobility of monomers in polymer fibers without NPs along radial and axial directions, respectively. For monomers at the center, $M_r/M_{r,0} \approx M_a/M_{a,0} \approx 1$. For monomers at the interfacial region, on the other hand, $M_r/M_{r,0} \approx 0.9$, thus implying that the presence of NPs decreases the mobility of

monomers at the interfacial region by about 10% along the radial direction.

When NPs are located mostly at the fiber center (i.e., when $\epsilon_{np} \geq 1.5\epsilon$), the mobility of monomers is decreased by 10% or more regardless of the monomer position and directions. Both $M_r/M_{r,0}$ and $M_a/M_{a,0}$ are about 0.9 in all cases. Such a decrease in the monomer mobility leads to a significant decrease in $\langle(\Delta x)^2(t)\rangle$ for $\epsilon_{np} \geq 1.5\epsilon$ (Fig. 10) and also to slow conformational relaxation and translation of polymers in the fiber. This should contribute to the increase in τ_b and the slowdown of the deformation kinetics of polymer fibers.

The mobility of monomers shows identical temperature dependence regardless of the position of monomers and the spatial arrangement of NPs. As T is decreased from 1 to 0.7, M_r and M_a are decreased by up to 40% (Fig. 11). This stands in contrast to the temperature dependence of τ_b and ΔE^\ddagger : τ_b is decreased with a decrease in T for NPs of $\epsilon_{np} = 1\epsilon$ while τ_b is increased with a decrease in T for NPs of $\epsilon_{np} = 2\epsilon$. This suggests that not the decrease in mobility but the change in ΔE^\ddagger should be responsible for the temperature dependence of τ_b .

We also estimate the end-to-end vector time correlation function [$P_{ete}(t) \equiv \frac{1}{2}(3\{\frac{\vec{e}(t) \cdot \vec{e}(t=0)}{|\vec{e}(t)||\vec{e}(t=0)|} - 1\})^2$], where $\vec{e}(t)$ is the end-to-end vector of a single chain at time t . The decay time (τ_{ete}) is defined as a time when $P_{ete}(t)$ decays to e^{-1} . As shown in Fig. 12, for given value of N , τ_{ete} increases sharply with an increase in the magnitude (ϵ_{np}) of the attractive

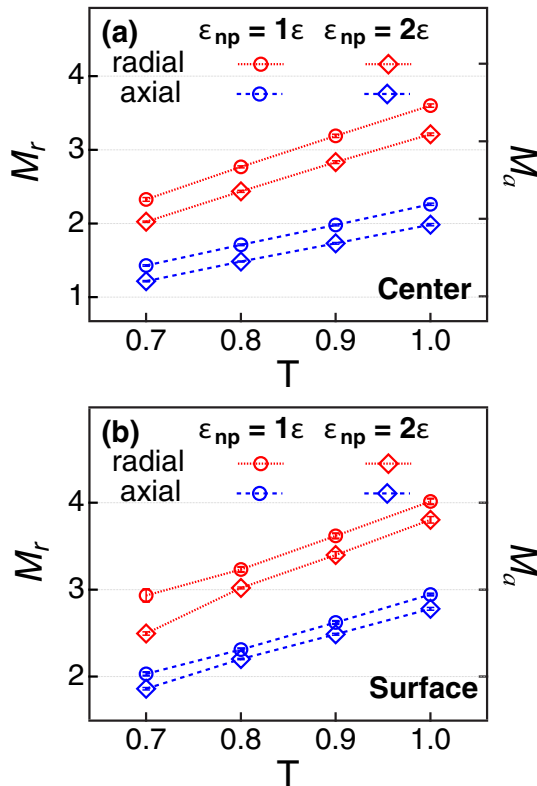


FIG. 11. The mobility of monomers as a function of T along radial (M_r , red) and axial (M_a , blue) directions (a) at the center and (b) the surface for $\epsilon_{np} = 1\epsilon$ (circle) and 2ϵ (diamond).

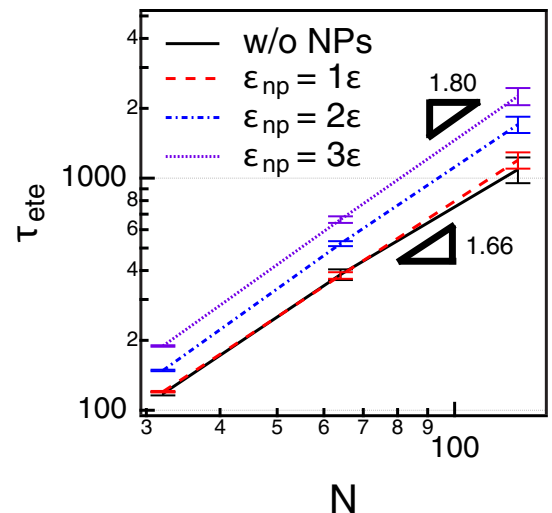


FIG. 12. The decay time (τ_{ete}) of the end-to-end vector auto-correlation functions of polymers as a function of the degree of polymerization (N).

interaction. Interestingly, a scaling relation holds between τ_{ete} and N , i.e., $\tau_{ete} \sim N^\alpha$. Scaling exponent (α) depends on the interaction strength between polymers and NPs. These suggest that adding NPs with attractive interactions into polymers of higher N will make the conformational relaxation of polymers quite slow.

IV. SUMMARY AND CONCLUSION

We perform molecular dynamics simulations to investigate the effects of NPs on the stability and the deformation kinetics of polymer fibers. We employ a coarse-grained but generic model for polymer fibers. We tune the diameter and the length of polymer fibers such that the polymer fibers are unstable and likely to deform spontaneously to polymer globules of smaller surface areas. We estimate the time (τ_b) taken for unstable polymer fibers to disrupt to polymer globules. Interestingly, when NPs are introduced to polymer fibers, τ_b is increased significantly and the polymer fibers become kinetically stable. For example, when the intermolecular interactions between NPs and polymers are quite attractive with $\epsilon_{np} = 2\epsilon$, most polymer fibers do not break down in our simulations at $T = 0.7$.

The deformation process might be divided into two regimes: regime 1 where polymer fibers begin to break down after crossing the free energy barrier (ΔF^\ddagger) and regime 2 where polymer fibers fluctuate before crossing the free energy barrier. We find that the length of regime 1 is independent of the presence and the type of NPs in the polymer fibers. On the other hand, the length of regime 2 depends strongly on the presence and the type of NPs, which should affect τ_b . τ_b is increased when NPs are introduced to polymer fibers. As the intermolecular interaction between polymers and NPs becomes more attractive, regime 2 becomes longer and τ_b is increased further, which indicates that the polymer fibers become more kinetically stable. This suggests that the addition of NPs would increase the free energy barrier (ΔF^\ddagger).

The interaction type of NPs affects the spatial arrangement of NPs within polymer fibers. When $\epsilon_{np} \geq 1.5\epsilon$ and the intermolecular interaction between NPs and polymers is sufficiently attractive, NPs are located at the central region of polymer fibers. On the other hand, when ϵ is relatively small and the interaction is repulsive, NPs are located at the interfacial region of polymer fibers. Such different spatial arrangement of NPs may lead to the different temperature dependence of τ_b . When $\epsilon_{np} \geq 1.5\epsilon$ and NPs are located at the fiber center, τ_b is increased with an increase in $1/T$, which suggests that ΔE^\ddagger should be positive. When $\epsilon_{np} < 1.5$ and NPs are located at the fiber surface, τ_b is decreased with an increase in $1/T$, which suggests that $\Delta E^\ddagger < 0$. Different spatial arrangement of NPs within polymer fibers seems to lead to different values of $\Delta E^\ddagger < 0$.

In a future study, we plan to investigate the effects of entanglement on the deformation kinetics and fiber stability. The polymer chain employed in this study is relatively short such that polymers do not entangle each other. When sufficiently long polymer chains are entangled, the viscosity and conformational relaxation time should be increased significantly, for which one may expect that the deformation kinetics would slow down significantly. The effects of entanglement on the deformation kinetics and glass transition of polymer fibers should be a topic of interest.

ACKNOWLEDGMENTS

This research was supported by the Basic Science Research Program through the National Research Foundation of Korea (NRF) funded by the Ministry of Education (2018R1A6A1A03024940). The authors would also like to acknowledge support from the KISTI supercomputing center through the strategic support program for supercomputing application research (Grant No. KSC-2014-C3-059).

-
- [1] S. Curgul, K. J. Van Vliet, and G. C. Rutledge, *Macromolecules* **40**, 8483 (2007).
 - [2] I. M. Radovic, D. B. Stojanovic, A. Kojovic, M. Petrovic, P. S. Uskokovic, V. J. Radojevic, and R. R. Aleksic, *J. Compos. Mater.* **51**, 3003 (2016).
 - [3] A. Arinstein, M. Burman, O. Gendelman, and E. Zussman, *Nat. Nanotechnol.* **2**, 59 (2007).
 - [4] C. Burger, B. S. Hsiao, and B. Chu, *Annu. Rev. Mater. Res.* **36**, 333 (2006).
 - [5] Y. Liu, S. Chen, E. Zussman, C. S. Korach, W. Zhao, and M. Rafailovich, *Macromolecules* **44**, 4439 (2011).
 - [6] Y. Li, C. T. Lim, and M. Kotaki, *Polymer* **56**, 572 (2015).
 - [7] E. P. S. Tan and C. T. Lim, *Compos. Sci. Technol.* **66**, 1102 (2006).
 - [8] M. H. Al-Saleh and U. Sundararaj, *Compos. Part A* **42**, 2126 (2011).
 - [9] K. H. Lee, H. Y. Kim, H. J. Bang, Y. H. Jung, and S. G. Lee, *Polymer* **44**, 4029 (2003).
 - [10] M. K. Shin, S. I. Kim, S. J. Kim, S.-K. Kim, H. Lee, and G. M. Spinks, *Appl. Phys. Lett.* **89**, 231929 (2006).
 - [11] S. Mohammadzadehmoghadam, Y. Dong, and I. Jeffery Davies, *J. Polym. Sci. Polym. Phys. Ed.* **53**, 1171 (2015).
 - [12] B. Tarus, N. Fadel, A. Al-Oufy, and M. El-Messiry, *Alexandria Eng. J.* **55**, 2975 (2016).
 - [13] S. Mazinani, A. Ajji, and C. Dubois, *Polymer* **50**, 3329 (2009).
 - [14] M. A. L. Manchado, L. Valentini, J. Biagiotti, and J. M. Kenny, *Carbon* **43**, 1499 (2005).
 - [15] R. Menini and M. Farzaneh, *Polym. Int.* **57**, 77 (2008).
 - [16] A. Alchalaby, R. Lwin, A. H. Al-Janabi, P. W. Trimby, S. C. Fleming, B. T. Kuhlmeier, and A. Argyros, *J. Lightwave Technol.* **34**, 2198 (2016).
 - [17] Y. Ji, C. Li, G. Wang, J. Koo, S. Ge, B. Li, J. Jiang, B. Herzberg, T. Klein, S. Chen, J. C. Sokolov, and M. H. Rafailovich, *Europhys. Lett.* **84**, 56002 (2008).
 - [18] M. D. Teli and R. D. Kale, *Polym. Eng. Sci.* **52**, 1148 (2012).
 - [19] W. K. Son, J. H. Youk, T. S. Lee, and W. H. Park, *Macromol. Rapid Commun.* **25**, 1632 (2004).
 - [20] K. Young, F. M. Blighe, J. J. Vilatela, A. H. Windle, I. A. Kinloch, L. Deng, R. J. Young, and J. N. Coleman, *ACS Nano* **4**, 6989 (2010).

- [21] Z.-M. Huang, Y. Z. Zhang, M. Kotaki, and S. Ramakrishna, *Compos. Sci. Technol.* **63**, 2223 (2003).
- [22] T.-C. Lin, J. Zhao, C. Cao, A. Javadi, Y. Yang, I. Hwang, and X. Li, *J. Micro Nano-Manuf.* **4**, 041008 (2016).
- [23] M. D'Amato, A. Dorigato, L. Fambri, and A. Pegoretti, *Express Polym. Lett.* **6**, 954 (2012).
- [24] L. Rayleigh, *Proc. R. Soc. London* **29**, 71 (1879).
- [25] S. Tomotika, *Proc. R. Soc. London A* **150**, 322 (1935).
- [26] J. Koplik and J. R. Banavar, *Phys. Fluids A* **5**, 521 (1993).
- [27] M. Moseler and U. Landman, *Science* **289**, 1165 (2000).
- [28] J. Fowlkes, S. Horton, M. Fuentes-Cabrera, and P. D. Rack, *Angew. Chem., Intl. Ed. Engl.* **51**, 8768 (2012).
- [29] R. Mead-Hunter, A. J. C. King, and B. J. Mullins, *Langmuir* **28**, 6731 (2012).
- [30] J. Eggers, *Phys. Rev. Lett.* **89**, 084502 (2002).
- [31] W. Kang and U. Landman, *Phys. Rev. Lett.* **98**, 064504 (2007).
- [32] N. Gopan and S. P. Sathian, *Phys. Rev. E* **90**, 033001 (2014).
- [33] D. J. Kirill, S. H. Davis, M. J. Miksis, and P. W. Voorhees, *Proc. R. Soc. London A* **455**, 3825 (1999).
- [34] Y.-C. Huang, P.-W. Fan, C.-W. Lee, C.-W. Chu, C.-C. Tsai, and J.-T. Chen, *ACS Appl. Mater. Interfaces* **5**, 3134 (2013).
- [35] M. M. Hohman, M. Shin, G. Rutledge, and M. P. Brenner, *Phys. Fluids* **13**, 2201 (2001).
- [36] X. Zong, K. Kim, D. Fang, S. Ran, B. S. Hsiao, and B. Chu, *Polymer* **43**, 4403 (2002).
- [37] S. Kawano, *Phys. Rev. E* **58**, 4468 (1998).
- [38] A. Tiwari, H. Reddy, S. Mukhopadhyay, and J. Abraham, *Phys. Rev. E* **78**, 016305 (2008).
- [39] D. K. Bhuptani and S. P. Sathian, *Phys. Rev. E* **95**, 053115 (2017).
- [40] A. N. Alexandrou, A. V. Bazilevskii, V. M. Entov, A. N. Rozhkov, and A. Sharaf, *Fluid Dyn.* **45**, 952 (2010).
- [41] N. Hoogesteijn von Reitzenstein, X. Bi, Y. Yang, K. Hristovski, and P. Westerhoff, *J. Appl. Polym. Sci.* **133**, 43811 (2016).
- [42] H. Im, Y. Oh, H. W. Cho, J. Kim, K. Paeng, and B. J. Sung, *Soft Matter* **13**, 5897 (2017).
- [43] A. Šarić, J. C. Pàmies, and A. Cacciuto, *Phys. Rev. Lett.* **104**, 226101 (2010).
- [44] A. Vahid, A. Šarić, and T. Idema, *Soft Matter* **13**, 4924 (2017).
- [45] J. C. Pàmies and A. Cacciuto, *Phys. Rev. Lett.* **106**, 045702 (2011).
- [46] R. A. Riggleman, J. F. Douglas, and J. J. de Pablo, *J. Chem. Phys.* **126**, 234903 (2007).
- [47] H. W. Cho and B. J. Sung, *Soft Matter* **13**, 1190 (2017).
- [48] A. Shavit and R. A. Riggleman, *Phys. Chem. Chem. Phys.* **16**, 10301 (2014).
- [49] R. A. Riggleman, K. Yoshimoto, J. F. Douglas, and J. J. de Pablo, *Phys. Rev. Lett.* **97**, 045502 (2006).
- [50] R. A. Riggleman, H.-N. Lee, M. D. Ediger, and J. J. de Pablo, *Soft Matter* **6**, 287 (2010).
- [51] K. Yoshimoto, T. S. Jain, K. van Workum, P. F. Nealey, and J. J. de Pablo, *Phys. Rev. Lett.* **93**, 175501 (2004).
- [52] D. M. Sussman, W.-S. Tung, K. I. Winey, K. S. Schweizer, and R. A. Riggleman, *Macromolecules* **47**, 6462 (2014).
- [53] D. M. Sussman, *Phys. Rev. E* **94**, 012503 (2016).
- [54] J. G. Park, G. T. Kim, V. Krstic, B. Kim, S. H. Lee, S. Roth, M. Burghard, and Y. W. Park, *Synth. Met.* **119**, 53 (2001).
- [55] Y. Zhou, M. Freitag, J. Hone, C. Staii, A. T. Johnson Jr., N. J. Pinto, and A. G. MacDiarmid, *Appl. Phys. Lett.* **83**, 3800 (2003).